Laser method of heating monolayer dusty plasmas

V. Nosenko* and J. Goree

Department of Physics and Astronomy,

The University of Iowa, Iowa City Iowa 52242

A. Piel

Institut für Experimentelle und Angewandte Physik,

Christian-Albrechts Universität, Kiel, Germany

(Dated: February 8, 2006)

Abstract

A method has been developed to heat and control temperature in a two-dimensional monolayer dusty plasma. A monolayer of highly charged polymer microspheres was suspended in a plasma sheath. The microspheres interacted with a Yukawa potential and formed a triangular lattice. Laser manipulation was used to apply random kicks to the particles. Two focused laser beams were moved rapidly around drawing Lissajous figures in the monolayer. The kinetic temperature of the particles increased with the laser power applied, and above a threshold a melting transition was observed. Characteristics of a thermal equilibrium of the laser-heated dusty plasma in solid and liquid states are discussed.

PACS numbers: 52.27.Lw, 82.70.Dd, 52.27.Gr

[1] Electronic mail: vladimir-nosenko@uiowa.edu

I. INTRODUCTION

Monolayer dusty plasmas are widely used in experiments. They offer a convenient model system to study wave propagation [1, 2], phase transitions [3], and transport phenomena [4] in solids and liquids. They are easy to produce and manipulate, and they allow direct imaging; the latter allows studying various phenomena at a kinetic level. Under usual experimental conditions, a monolayer dusty plasma tends to form a highly ordered triangular lattice of dust particles. In many experiments with monolayer dusty plasmas in a crystallized and especially liquid state, it is very important to be able to reliably control their temperature. However, there are only a few papers where the experimenters were able to control deliberately the temperature of a monolayer suspension of particles. In Ref. [5], a laser method was introduced for heating clusters of particles suspended in a plasma. In Ref. [2], a monolayer dusty plasma was heated by fast particles that moved around in an incomplete perturbation layer beneath the particle suspension. In this paper, we use a laser manipulation method comparable to that of Ref. [5], to heat and control the temperature of a bigger monolayer suspension of particles that had a size and number of particles typical for monolayer dusty plasma experiments. We discuss in detail the characteristics of the laser-heated dusty plasma in solid and liquid states and how it approximates a thermal equilibrium. In the course of this experiment, we melt a two-dimensional solid. We note that two-dimensional melting is believed to be mediated by the proliferation of defects, and there are various competing theoretical models and empirical descriptions of how this occurs [3, 6–12].

II. EXPERIMENTAL METHOD

We used the experimental setup of Fig. 1. A plasma was produced using a capacitively-coupled rf discharge. We used 35 W of rf power at 13.56 MHz, with an amplitude of 144 V peak-to-peak. The self-bias voltage was −89 V. To reduce the damping rate, we used Ar at a pressure of only 5 mTorr, corresponding to a gas drag, which is accurately modeled [13] by the Epstein expression, of $\nu = 0.87\ \mathrm{s}^{-1}$. The gas was in good thermal contact with the metal vacuum chamber, which was at room temperature.

A monolayer of microspheres was suspended in the plasma. The particles had a diameter

of 8.09 ± 0.18 μm [13] and a mass $m = 4.2 \times 10^{-13}$ kg. The particle suspension's diameter was $50 - 60$ mm. The interparticle potential for particles arranged in a single plane, like ours, was experimentally shown [14] to be nearly Yukawa: $U(r) = Q(4\pi\epsilon_0 r)^{-1}\exp(-r/\lambda_D)$, where Q is the particle charge and λ_D is the screening length. (This should not be confused with multiple-layer suspensions of particles, which form quasi-2D arrangements of particle chains [15] and might have a different potential.) The particle suspension is characterized by screening parameter $\kappa = a/\lambda_D$ and coupling parameter $\Gamma = Q^2/4\pi\epsilon_0 akT$, where T is the particle kinetic temperature. For liquids, the characteristic length is the 2D Wigner-Seitz radius $a = (\pi n)^{-1/2}$, where n is the areal number density [16]; it is related to the lattice constant b for a perfect triangular lattice by $a = (\sqrt{3}/2\pi)^{1/2}b$. We use the same definition of Γ as in recent theoretical studies of 2D Yukawa liquids [16] [17]. Other authors [18, 19] compute Γ using the mean interparticle distance as the length unit. We used the pulse technique of Ref. [20], making use of a theoretical wave dispersion relation, to measure $\kappa = 0.43 \pm 0.06$ and $Q = -12\ 800 \pm 1200e$.

Initially, our suspension was an undisturbed triangular lattice, Fig. 2(a). As is typical for a 2D monolayer with our experimental conditions, it had a highly ordered state. The static structure factor $S(\mathbf{k})$ in the inset has the distinctive peaks of a hexagonal crystal, and the pair correlation function $g(r)$, Fig. 2(b), has many peaks and a correlation length of $r_{\rm corr} = 25a$.

The particles were imaged through the top window by a video camera. We digitized movies of 2048 frames at 29.97 frames per second. The 22.7×17.0 mm^2 field of view included ≈ 1100 particles, Fig. 2(a). Coordinates x, y and velocities u_x, u_y were then calculated with subpixel resolution [21] for each particle in each frame. As an indication of our measurement resolution, we note that a particle with a velocity of 1 mm/s would be displaced almost exactly one pixel per frame. Additionally, using a side-view camera we verified that no out-of-plane buckling occurred; we can therefore state that all experimental results reported here are for a single horizontal layer of particles.

We used laser manipulation to heat our suspension of particles, Fig. 1. Two laser beams are pointed toward the suspension from opposite sides at a grazing angle of $6.2 - 7.2^\circ$ with respect to a horizontal plane. Particles are pushed by the radiation pressure force, which was verified [13] to be proportional to the incident laser intensity. The beam of a 532 nm solid-state laser was split in two. At their foci at the particle location, the laser beams had a full

width at half maximum of $2W = 0.25$ mm and together a maximum total power of 10.55 W. Due to the grazing angle of incidence, each laser beam made an elliptical footprint on the particle suspension; this footprint was elongated by a factor of about 8.6 in the x direction as compared to the y direction. During laser manipulation, the laser power remained constant.

The laser beams were moved about by pointing them in varying directions using scanning mirrors. The point (x, y) at which a laser beam struck the suspension was rastered about using a nearly triangular waveform with the amplitude of A_x and frequency f_x in the x direction and respectively A_y and f_y in the y direction. As a result, each laser beam was rastered in a Lissajous figure. The amplitudes A_x and A_y determine the size $2A_x$ by $2A_y$ of the rectangular laser-heated stripe. Unlike in an earlier experiment with a small-diameter cluster [5], we did not manipulate the entire particle suspension. The scanning frequencies were different for the beam motion in the x and y directions, $f_x = 9$ Hz and $f_y = 14.5623$ Hz respectively. The two Lissajous frequencies f_x and f_y were chosen so that their ratio was close to an irrational number $f_x/f_y \approx (\sqrt{5}-1)/2$. This helped to avoid frequent repetitions in the Lissajous pattern and hence improved the desired randomization of the kicks. We varied the lower frequency, while maintaining a constant ratio of the two frequencies, and we found that the observable heating effect was significantly decreased when the lower frequency was higher than 20 Hz. This suggests that the heating method is most effective when the lower of the two frequencies is within the range of frequencies allowed by the dispersion relation, as we will show later in this paper. We used the same pair of frequencies but an arbitrary phase for both laser beams. This scheme provided brief intense random kicks to the particles. As a result, their mean kinetic energy increased.

We can estimate how intense and infrequent the kicks were, depending on the laser beam parameters. Because the beam's footprint was elongated in the x direction, the time duration τ_{kick} that a particle was exposed to a moving laser beam was determined primarily by the beam's width $2W$ in the y direction. The velocity of the beam in the y direction was $4f_yA_y$, so that the duration of a kick is characterized by $\tau_{\text{kick}} = W/2f_yA_y$. For our parameters, including a width $2A_y = 12.4$ mm for the laser-heated stripe, $\tau_{\text{kick}} \approx 0.7$ ms. To estimate a typical time interval τ_{relax} during which a particle does not experience a kick, we can approximate with good accuracy that the ratio $\tau_{\text{kick}}/(\tau_{\text{relax}} + \tau_{\text{kick}})$ is equal to the ratio of the areas of the laser footprint $\pi W^2/\sin 6.7^\circ$ and the area of the heated region $4A_xA_y$. We thus find, for our laser beam parameters, $\tau_{\text{kick}}/\tau_{\text{relax}} \approx 4.5 \times 10^{-4}$, and $\tau_{\text{relax}} \approx 1.6$ s.

Our method of laser heating is comparable to that of Ref. [5]. The differences as compared to Ref. [5] are as follows. First, we used two laser beams of the same power coming from opposite sides. This resulted in zero net momentum introduced into the suspension by the laser beams. Second, in our experiment the laser beams struck the lattice at a grazing angle of $6.2 - 7.2^\circ$ with respect to a horizontal plane. As a result, only those particles that happened to be in the elliptical footprint of the laser beam were pushed at a given time. Third, we used Lissajous figures for the laser beam trajectories rather than random waveforms. This makes it convenient to heat uniformly a rectangular stripe in the particle suspension. Fourth, we used a much bigger suspension that consisted of ≈ 6700 particles. This number of particles is typical for experiments where waves and transport phenomena in dusty plasmas are studied.

III. RESULTS

By varying the output power of our manipulation laser, we were able to control the mean kinetic energy of the particles. As the mean kinetic energy increased to a certain point the suspension melted and became liquid. By increasing the laser power still further, we heated the resulting liquid. Below we will discuss in detail the effects of laser heating on the particle suspension.

A. Particle suspension in solid and liquid states

Two extreme states of our particle suspension are shown in Fig. 2. If undisturbed, the suspension is in a solid state that is a highly ordered triangular lattice with hexagonal symmetry, Fig. 2(a). At a high excitation laser power of 8.20 W, the suspension is in a liquid state, Fig. 2(c). The liquid-like order of the particle suspension is indicated by the diffusiveness of the structure factor $S(\mathbf{k})$ in the inset in Fig. 2(c). The pair correlation function in Fig. 2(d) has only 3 or 4 maxima and the amplitude of the first maximum is as low as 2.31, which is characteristic of a liquid state.

To study the melting transition from the solid to the liquid state, we calculate three parameters: the pair correlation function $g(r)$, static structure factor $S(\mathbf{k})$, and coupling parameter Γ of the particle suspension. Repeating these calculations for every setting of

the excitation laser power yields the results shown in Fig. 3. We will describe later in this paper how we calculated the values of Γ. We found that $S(\mathbf{k})$ has hexagonal features that are increasingly blurred as laser power is increased from 0 W to 1.76 W. At higher powers, the structure factor has a diffuse appearance with visible rings, for laser power from 2.34 W up to 10.55 W. We conclude that in the range of excitation laser power of $0 - 1.76$ W our suspension is in an increasingly disordered solid state and in the range of $2.34 - 10.55$ W it is in a liquid state. The suspension melts somewhere between 1.76 W and 2.34 W of excitation laser power. Based on our other parameters, the melting occurs for a coupling parameter Γ_x in the range of $128 - 206$, Γ_y in the range of $158 - 281$, and an amplitude of the first peak of $g(r)$ in the range of $3.08 - 3.81$. These observations are consistent with the results of molecular dynamics simulation of the melting of 2D Yukawa systems [17]. To study the melting transition in more detail, more data points between 1.76 W and 2.34 W of excitation laser power would be required; we did not measure these in the present paper.

B. Kinetic temperature of the particles

To study the effect of laser heating on the particle suspension in the solid and liquid states, we analyze the particle velocity distribution functions. In Fig. 4, the distribution functions are shown for three different levels of the heating laser power.

In an undisturbed lattice that was in a crystalline state, the distribution function was Maxwellian, as shown by the straight lines over four decades in the logarithmic plots of particle counts vs. v^2, in Fig. 4(a). The only deviation from a Maxwellian distribution is a sharp rise of the v_y curve at $v_y \approx 0$. We observed this feature in the distributions of v_y at all values of the heating laser power in Fig. 4. (In preparing the histogram in Fig. 4(a), we selected time series with no intermittent episodes when the average particle energy was momentarily elevated, which sometimes occurred due to the movement of a distant defect that was not in the field of view of the camera. This was done only for the crystalline state of Fig. 4(a).)

At a low heating laser power, for which the lattice was in a slightly disordered crystalline state, the particle velocity distribution function was also Maxwellian, though the v_y distribution somewhat deviated from Maxwellian for higher velocities. Note that the slope of the v_y distribution is steeper than for v_x, indicating a lower kinetic temperature in the y direction;

this is an indication of an anisotropic heating, as we will discuss later in this section.

At a high heating laser power, as the particle suspension was in a liquid state, the distribution functions for v_x and v_y became rather different. The v_x distribution was Maxwellian over three decades of particle count. The v_y distribution was also Maxwellian on average, but additionally it had two prominent peaks at low velocities and wavy features elsewhere.

We attribute the latter features in the v_y distribution, including the sharp rise at $v_y \approx 0$, to artifacts arising from the well-known problem of pixel locking [22, 23]. The pixel-locking effect arises when the sub-pixel position of a particle is calculated using a particle image where the particle is represented by only a few pixels. Usually pixel locking causes the computed particle positions to have systematic errors, with certain computed particle positions occurring more frequently than others. The problem becomes more severe as the particle image becomes smaller and fills fewer pixels. When the image of the particle has a width of only two or three pixels, the computed position has its most probable values spaced at one-pixel intervals [23]. Due to the analog video camera we used, the particle images had an elliptical shape with an average size of 4.8 ± 1.1 pixel in the x direction and 2.9 ± 0.8 pixel in the y direction. Therefore, the pixel-locking problem was most severe for the y components of the particle positions and velocities, leading to the spurious peaks in the distribution of v_y. These peaks appear at velocities corresponding to a particle displacement of one pixel per frame, and integer multiples of this value, as most clearly seen in Fig. 4(c).

Pixel-locking artifacts could affect other experiments more adversely than the one reported here. In general, experimenters may find it useful to perform tests of their images to determine the extent of pixel locking. In addition to checking the velocity distribution function as shown here, as another test we also computed the distribution of particle positions relative to pixel boundaries. We found that these tests are useful in choosing the value for the gray-scale threshold that is applied to bit-map images in the step just before particles are identified. Varying this threshold to an optimum level allows one to reduce the pixel-locking effect. Another test, which we did not perform, would be rotating the camera 90° degrees during the experiment.

Aside from the artifacts created by pixel locking, the v_x distribution was Maxwellian for all velocities, and the v_y distribution was Maxwellian on average, for all values of the heating laser power that we used. This means that we can reasonably characterize the particle motion by a certain temperature at every value of the heating laser power. We calculated

the particle temperature from the second moments of the particle velocity distributions using the formula $T_{x,y} = m\langle(v_{x,y} - \overline{v}_{x,y})^2\rangle/k_B$, where m is the particle mass and k_B is the Boltzman constant.

The kinetic temperature is different in the x and y directions, i.e., it is anisotropic. It is higher in the x direction, where we introduced momentum by pushing the particles by laser beams, and lower in the y direction, where the particles attained momentum only by collisions with other particles.

As an additional test of how close our particle suspension was to a thermal equilibrium we found that to a certain degree we achieved an equipartition of particle kinetic energy in frequency space. A system in thermal equilibrium would have a velocity power spectrum that would have two key qualities: it should be broadband without significant energy concentrated in peaks at specific frequencies, and it should be flat up to a certain frequency. Shown in Fig. 5 are the power spectra $v_x(f)$ and $v_y(f)$ of the particle velocity. Both $v_x(f)$ and $v_y(f)$ have a baseline that is flat within a factor of two from 0 Hz to 10 Hz and then declines significantly from 10 Hz to 15 Hz. Superimposed on this baseline are peaks corresponding to the combination frequencies of the Lissajous frequencies f_x and f_y (see Table I). The fraction of power within these spectral peaks is 18% of the total power. This means that the energy that is introduced into our system at various combination frequencies of f_x and f_y is scattered rather efficiently into phonons with a broad spectrum represented by the baseline in Fig. 5. Note that while f_y lies outside of the phonon spectrum, f_x was chosen slightly within it. This provides for increased efficiency of coupling energy into our particle suspension.

The kinetic temperature of our particle suspension depended on the heating laser power, Fig. 6(a). For low laser powers up to 3.52 W, this dependence is described well by a power law with the exponent of 1.67 for T_x and 2.0 for T_y. This result is comparable to the quadratic dependence predicted by the one-particle model of Ref. [5]. In the intermediate range of laser power from 3.52 W to 8.20 W, the temperature dependence is also described well by a power law, but the best values for the exponent are 0.55 for T_x and 0.36 for T_y. Finally, for laser powers higher than 8.20 W, the particle temperature unexpectedly declined with increasing laser power. One possible explanation of this observation is due to the change of the laser beam's shape for powers higher than 8.20 W. At high power, the laser beam's transverse profile departed from a Gaussian mode and developed a donut-like mode. As a

result of this change, the laser beam might have become defocused, and that in turn might have resulted in less efficient heating of the particles.

In Fig. 6(b), the coupling parameter Γ of the particle suspension is shown as a function of the laser power applied. To calculate the values of Γ, the temperature data from Fig. 6(a) were used.

A conspicuous feature seen in Fig. 6 is an anisotropy of the particle temperature: $T_x > T_y$ at all values of the heating laser power. This is explained by the anisotropy of our heating method. The particles were pushed by the laser beams in the $\pm x$ directions only. Whatever momentum particles acquired in the y direction was acquired by collisions with other particles.

C. Spatial distribution of the particle temperature

The spatial distribution of the particle temperature was rather homogeneous inside the laser-heated stripe, for a low laser power up to 3.52 W. Shown in Fig. 7 are spatial profiles of the particle temperature $T_x(y)$ and $T_y(y)$, measured in the direction transverse to the laser beams while averaging over the parallel direction x. For a laser power up to 3.52 W, the $T_x(y)$ profiles are more or less flat, with a superimposed oscillatory structure inside the laser-heated stripe, and a sharp decline outside of it, Fig. 7(a). The $T_y(y)$ profiles are nearly flat and rather smooth inside the laser-heated stripe, and they gradually decline outside of it, Fig. 7(b). For a laser power higher than 3.52 W, the $T_x(y)$ profiles developed a substantial oscillatory pattern similar to that at low power but with a higher magnitude. This oscillatory structure in $T_x(y)$ is a typical result in our laser-heating experiments. The cause of this structure is undetermined, but it may be due to the interference of the Lissajous trajectories of the heating laser beams. The $T_y(y)$ profiles for high laser power were similar to those for low laser power; they were smooth but less flat. We conclude that particle collisions, which can channel energy from the x into the y direction, are efficient at eliminating sharp structures from the spatial distribution of $T_y(y)$.

D. Characteristics of thermal equilibrium

As we have shown above, several properties of our laser-heated suspension approximate those of a system in thermal equilibrium. Those properties are the velocity distribution function, wave energy equipartition, and spatial uniformity. In this section, we will discuss the results of one more test of thermal equilibrium. This is the same test used to qualify software thermostats for molecular dynamics simulations [24]. We started by calculating the instantaneous temperature of our system at every time step. We computed $T_{x,y} = m\langle(v_{x,y} - \overline{v}_{x,y})^2\rangle/k_B$ for all N particles inside the laser-heated stripe in every frame of our 2048-frame movies. This computed value of the temperature varied randomly, from one frame to the next, due to the finite number N of particles that were imaged. We then calculated the experimental temperature fluctuation $\delta T^{\rm exp}$ as the rms variation of the time series of instantaneous temperatures. We compare $\delta T^{\rm exp}$ to the canonical temperature fluctuation of a system in thermal equilibrium $\delta T^{\rm canon} = \overline{T}(2/N)^{1/2}$. The ratio of $\delta T^{\rm exp}$ to $\delta T^{\rm canon}$ is shown in Fig. 8. The ideal value of this ratio, for a system in the thermal equilibrium, is unity. Over a wide range of particle temperature, our experimental temperature fluctuation exceeds the canonical fluctuation by a factor of $1.5-2.1$ for T_x and $1.1-1.9$ for T_y. This is a favorable result because it is comparable to the ratio of 1.1 achieved in molecular dynamics simulations using the excellent Nosé-Hoover software thermostat [25]. This adds to the list of the properties of our system showing how closely it approximates a system in thermal equilibrium.

IV. SUMMARY

To summarize, a method was developed to heat and control temperature in a two-dimensional monolayer dusty plasma. Two counter-propagating laser beams are used to apply brief intense kicks to particles suspended as a monolayer in a plasma. The beams strike the particle suspension at a grazing angle and move about to draw Lissajous figures on the suspension. The ratio of the Lissajous frequencies is chosen close to an irrational number so that the Lissajous pattern covers the rectangular heated region virtually without repeating itself. This improves the desired randomization of the kicks.

To verify that our laser-heated particle suspension has properties that approximate those

of a system in thermal equilibrium, a number of tests was performed. First, the particle velocity distributions were on average Maxwellian for the laser-heated suspension. We observed non-Maxwellian features in the distribution of the transverse velocity but we identified these as artifacts arising due to pixel-locking effect. Second, the particle kinetic energy was partitioned rather uniformly in the frequency domain, with 82% of the energy in the broadband spectrum and 18% in coherent peaks. Third, the spatial distribution of the particle temperature was rather homogeneous in the region that was heated, except for high laser powers. Fourth, the particle temperature fluctuation was comparable to that of a canonical system at equilibrium.

Unlike systems in thermal equilibrium, however, our laser-heated particle suspension has an anisotropic temperature. The temperature is higher in the x direction where the particles receive kicks from the laser beams. To improve isotropy in the temperature, two more laser beams could be added along the y axis, so that particles get random kicks in the $\pm y$ directions as well as $\pm x$ directions.

V. ACKNOWLEDGMENTS

We thank F. Skiff for valuable discussions. This work was supported by NASA and the U.S. Department of Energy, and A.P. acknowledges financial support by DFG under contracts Pi185/25-1 and SFB TR-24/A2.

---

[1] V. Nosenko, K. Avinash, J. Goree, and B. Liu, Phys. Rev. Lett. **92**, 085001 (2004).

[2] S. Nunomura, S. Zhdanov, D. Samsonov, and G. Morfill, Phys. Rev. Lett. **94**, 045001 (2005).

[3] R.A. Quinn and J. Goree, Phys. Rev. E **64**, 051404-1 (2001).

[4] V. Nosenko and J. Goree, Phys. Rev. Lett. **93**, 155004 (2004).

[5] M. Wolter and A. Melzer, Phys. Rev. E **71**, 036414 (2005).

[6] J.M. Kosterlitz and D.J. Thouless, J. Phys. C **6**, 1181 (1973).

[7] B.I. Halperin and D.R. Nelson, Phys. Rev. Lett. **41**, 121 (1978).

[8] A.P. Young, Phys. Rev. B **19**, 1855 (1979).

[9] S.T. Chui, Phys. Rev. Lett. **48**, 933 (1982).

FIG. 1: Experimental apparatus. Polymer microspheres levitate above the lower electrode in a capacitively coupled rf plasma. The particles settle in a horizontal monolayer, arranged in a triangular crystalline lattice. The particles are heated by giving them brief intense kicks with two counter-propagating laser beams that draw Lissajous figures on the particle suspension. The lattice can be melted using this heating method.

FIG. 2: Monolayer particle suspension in a crystalline state (a),(b) and in liquid state (c),(d). The snapshot of an undisturbed suspension (a) shows a highly ordered triangular lattice. The particle trajectories (c) are rather involved inside the laser-heated stripe, in a liquid state. Insets in (a) and (c) show the static structure factor $S(\mathbf{k})$ calculated as in Ref. [4]. Corresponding pair correlation functions $g(r)$ are shown in panels (b) and (d). The spatial region included in the calculations of $g(r)$ was the heated stripe $3.6 < y < 12$ mm.

[10] S.T. Chui, Phys. Rev. B **28**, 178 (1983).

[11] M.A. Glaser and N.A. Clark, Adv. Chem. Phys. **83**, 543 (1993).

[12] S. Toxvaerd, Phys. Rev. A **24**, 2735 (1981).

[13] B. Liu, J. Goree, and V. Nosenko, Phys. Plasmas **10**, 9 (2003).

[14] U. Konopka, G.E. Morfill, and L. Ratke, Phys. Rev. Lett. **84**, 891 (2000).

[15] W.-Y. Woon and L. I, Phys. Rev. Lett. **92**, 065003 (2004).

[16] G.J. Kalman, P. Hartmann, Z. Donkó, and M. Rosenberg, Phys. Rev. Lett. **92**, 065001 (2004).

[17] P. Hartmann, G.J. Kalman, Z. Donkó, and K. Kutasi, Phys. Rev. E **72**, 026409 (2005).

[18] O. Vaulina, S. Khrapak, and G. Morfill, Phys. Rev. E **66**, 016404 (2002).

[19] V.E. Fortov, O.S. Vaulina, O.F. Petrov *et al.*, Phys. Rev. Lett. **90**, 245005 (2003).

[20] V. Nosenko, J. Goree, Z.W. Ma, and A. Piel, Phys. Rev. Lett. **88**, 135001 (2002).

[21] D. Samsonov, J. Goree, Z.W. Ma, and A. Bhattacharjee, Phys. Rev. Lett. **83**, 3649 (1999).

[22] M. Shimizu and M. Okutomi, International Journal of Computer Vision **63**, 207 (2005).

[23] H. Nobach and M. Honkanen, Experiments in Fluids **38**, 511 (2005).

[24] B. Holian, A. Voter, and R. Ravelo, Phys. Rev. E **52**, 2338 (1995).

[25] B. Liu, private communication (2004).

FIG. 3: Three characteristics that we use to distinguish between solid and liquid states of the particle suspension: coupling parameter Γ (vertical axis), the amplitude of the first peak of pair correlation function $g(r)$ (horizontal axis), and the static structure factor $S(\mathbf{k})$ (two insets). We find that the lattice melts between 1.76 W and 2.34 W of heating laser power.

FIG. 4: Particle velocity distributions for an undisturbed lattice (a) and the particle suspension that was heated using low laser power of 0.59 W (b) and high laser power of 8.20 W (c). In the laser-heated suspension, the velocity distribution is Maxwellian in the x direction and it is also Maxwellian on average in the y direction. A Maxwellian fit is shown by the straight lines. We attribute the peaks and wavy features in the distribution of v_y to artifacts due to pixel-locking effect. The particle kinetic temperature was calculated as $T_{x,y} = m\langle(v_{x,y} - \overline{v}_{x,y})^2\rangle/k_B$, where m is the particle mass and k_B is the Boltzman constant. The spatial region included in these calculations was a rectangular region $3.6 < y < 12$ mm slightly narrower than the width of the heated stripe.

FIG. 6: Particle kinetic temperature T (a) and Coulomb coupling parameter Γ (b) as a function of the heating laser power. We attribute the temperature decline for the laser powers higher than 8.20 W to a change in the shape of the laser beams.

FIG. 7: Spatial profiles of the particle kinetic temperature. The profiles are calculated in the direction transverse to the laser beams while averaging in the parallel direction. The temperature is rather homogeneous inside the laser-heated stripe, except for high laser powers.

FIG. 5: Power spectra of the particle velocity in the direction of the laser beams (solid line), and in the transverse direction (dashed line). Two Lissajous frequencies f_x and f_y are indicated by arrows. Spectral peaks correspond to various combination frequencies of f_x and f_y, Table I. Baseline represents the spectrum of phonons excited in the particle suspension. The energy that was initially coupled into the system at the combination frequencies of f_x and f_y is efficiently distributed over broad phonon spectra.

FIG. 8: Fluctuation of the particle kinetic temperature normalized by the fluctuation of a canonical system in thermal equilibrium. In a wide range of temperature, their ratio is $1.7 - 2.1$ for T_x and $1.1 - 1.6$ for T_y. This is comparable to the ratio of 1.1 achieved in molecular dynamics simulations using the Nosé-Hoover software thermostat [25].

TABLE I: Combination frequencies in the power spectrum of Fig. 5.

peak (Hz)	combination frequency
0.811	$\lvert 8f_x - 5f_y \rvert$
1.313	$\lvert 5f_x - 3f_y \rvert$
2.125	$\lvert 3f_x - 2f_y \rvert$
2.626	$\lvert 10f_x - 6f_y \rvert$
2.936	$\lvert 11f_x - 7f_y \rvert$
3.438	$\lvert 2f_x - 3f_y \rvert$
3.748	$\lvert 19f_x - 12f_y \rvert$
4.751	$\lvert 7f_x - 4f_y \rvert$
5.061	$\lvert 14f_x - 9f_y \rvert$

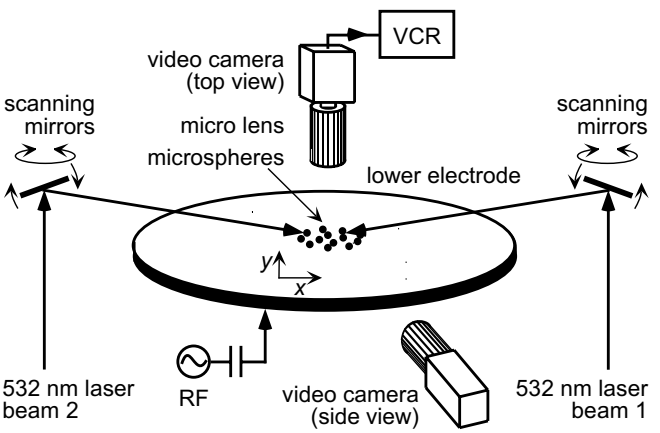
VCR
video camera
(top view)
scanning
mirrors
micro lens
microspheres
lower electrode
scanning
mirrors
y
x
532 nm laser
beam 2
RF
video camera
(side view)
532 nm laser
beam 1

Fig. 1

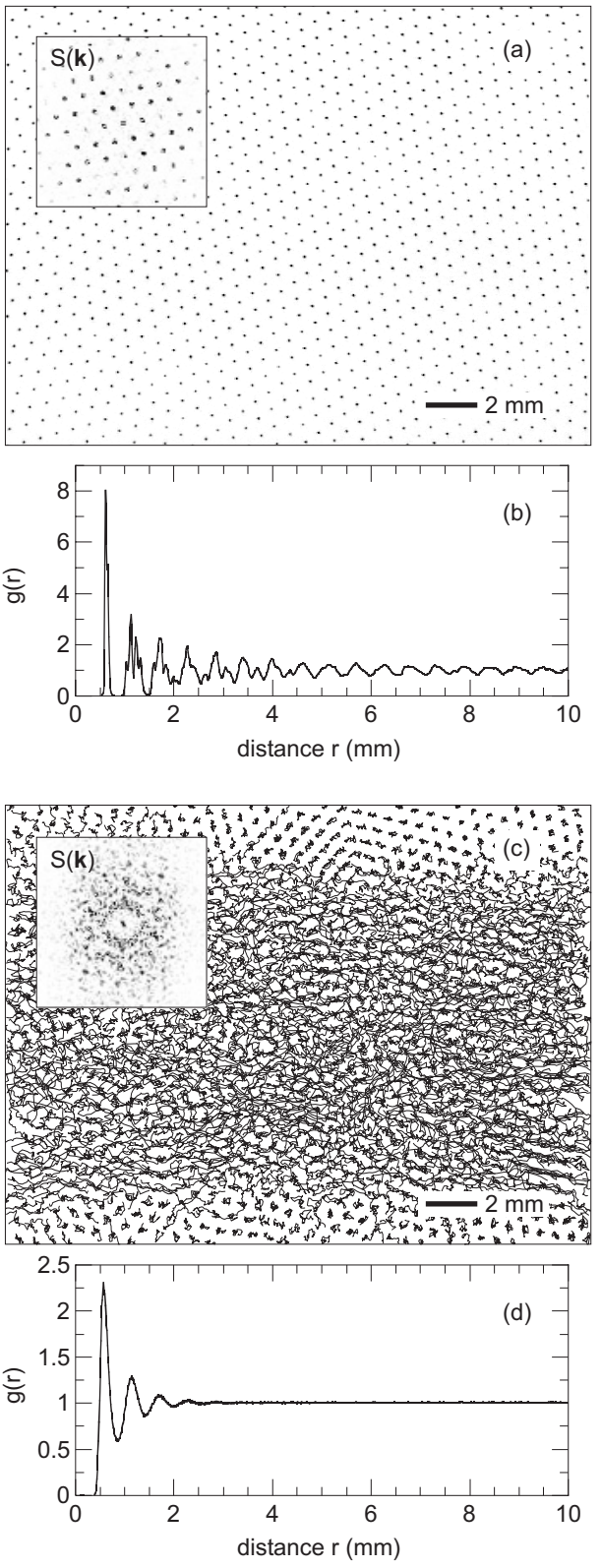

Fig. 2

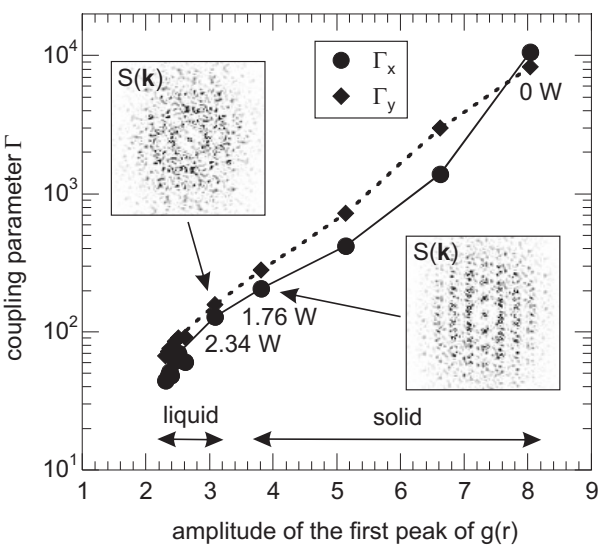
coupling parameter Γ
amplitude of the first peak of g(r)
10^4
10^3
10^2
10^1
1
2
3
4
5
6
7
8
9
S(**k**)
Γ_x
Γ_y
0 W
1.76 W
2.34 W
S(**k**)
liquid
solid

Fig. 3

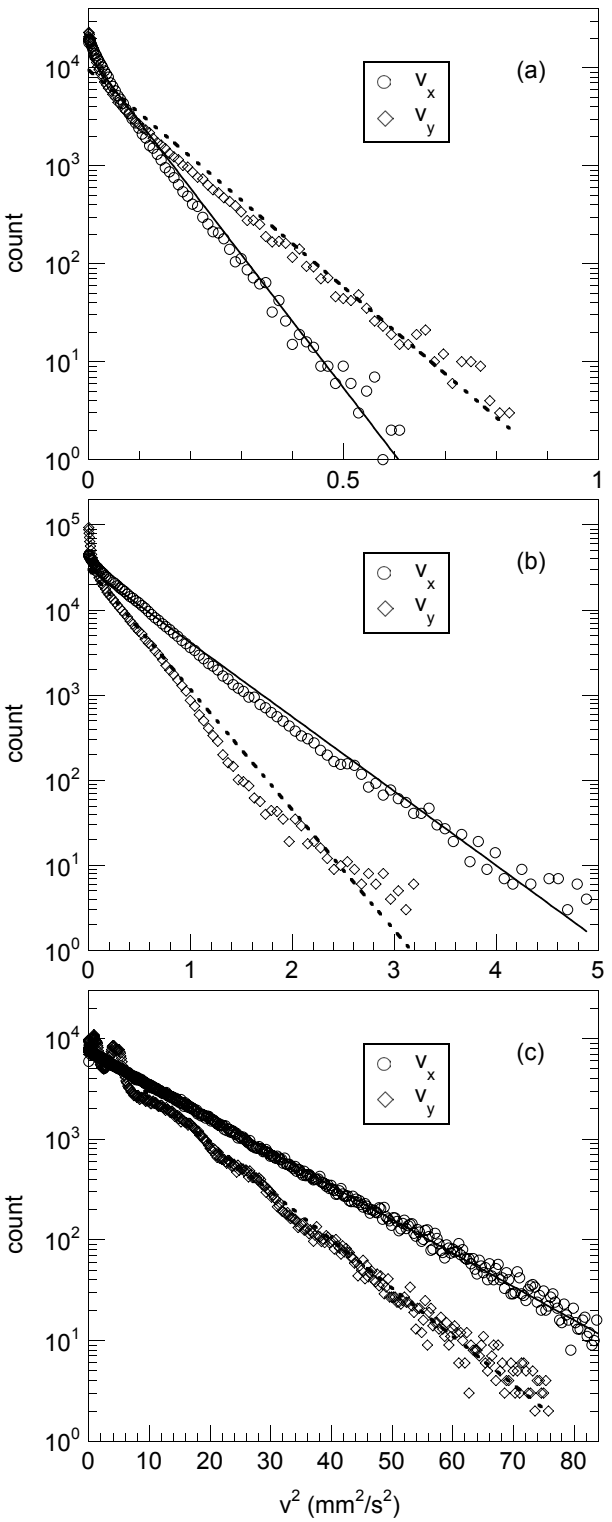

Fig. 4

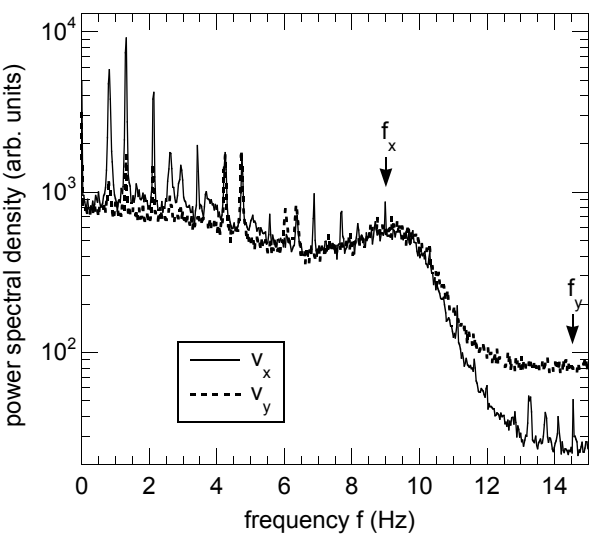
power spectral density (arb. units)
frequency f (Hz)
10^4
10^3
10^2
0
2
4
6
8
10
12
14
f_x
f_y
v_x
v_y

Fig. 5

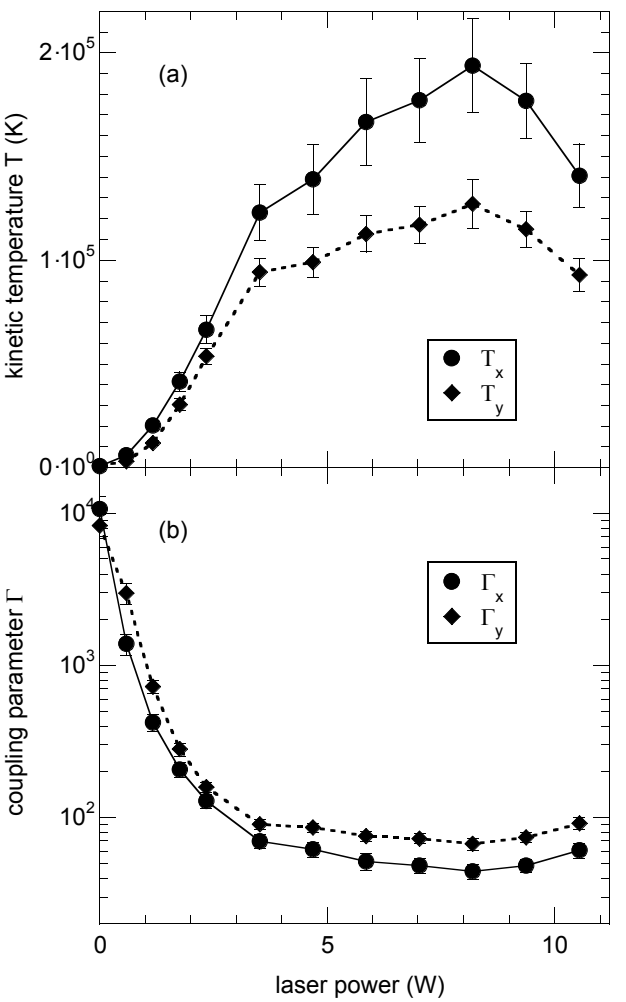
(a)
(b)
kinetic temperature T (K)
coupling parameter Γ
laser power (W)
T_x
T_y
Γ_x
Γ_y
2·10^5
1·10^5
0·10^0
10^4
10^3
10^2
0
5
10

Fig. 6

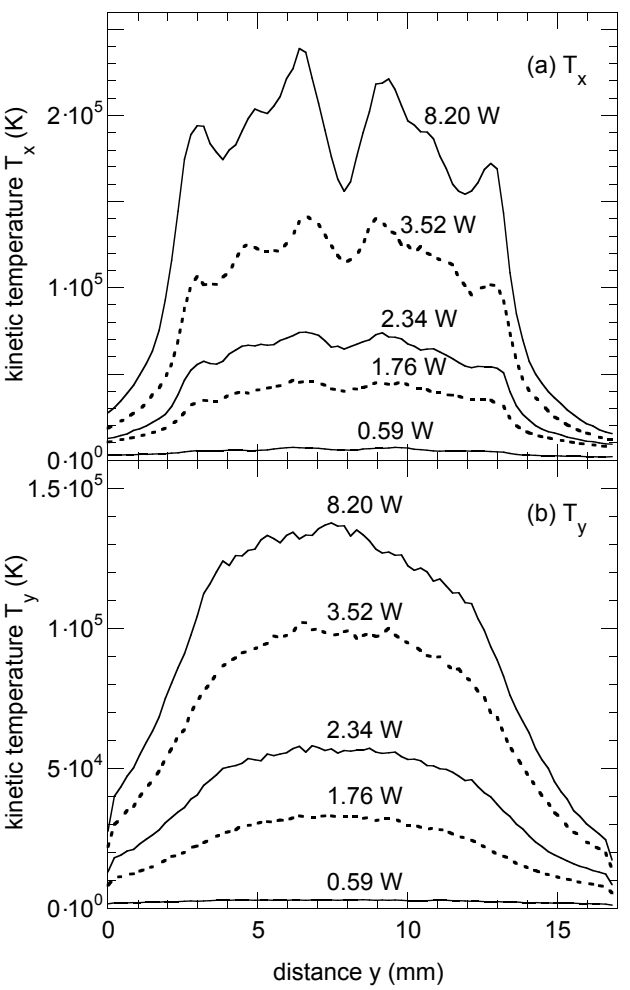
(a) T_x
8.20 W
3.52 W
2.34 W
1.76 W
0.59 W
kinetic temperature T_x (K)
$2 \cdot 10^5$
$1 \cdot 10^5$
$0 \cdot 10^0$
(b) T_y
8.20 W
3.52 W
2.34 W
1.76 W
0.59 W
kinetic temperature T_y (K)
$1.5 \cdot 10^5$
$1 \cdot 10^5$
$5 \cdot 10^4$
$0 \cdot 10^0$
0
5
10
15
distance y (mm)

Fig. 7

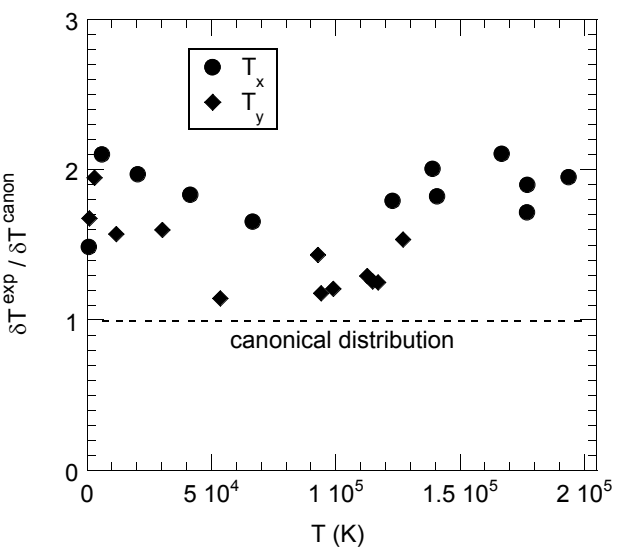
3
2
1
0
T_x
T_y
canonical distribution
$\delta T^{exp} / \delta T^{canon}$
0
5 10^4
1 10^5
1.5 10^5
2 10^5
T (K)

Fig. 8